Current Applied Physics 45 (2023) 53–63

Contents lists available at ScienceDirect

Current Applied Physics

journal homepage: www.elsevier.com/locate/cap

Cu and Mn centered nicotinamide/nicotinic acid complexes for interlayer of Schottky photodiode

Adem Kocyigit [a,*], Dilber Esra Yıldız [b,**], Ali Akbar Hussaini [c], Dursun Ali Kose [d], Murat Yıldırım [c]

[a] Bilecik Seyh Edebali University, Vocational High School, Department of Electronics and Automation, 11230, Bilecik, Turkey
[b] Hitit University, Faculty of Arts and Sciences, Department of Physics, 19030, Corum, Turkey
[c] Selcuk University, Faculty of Science, Department of Biotechnology, 42130, Konya, Turkey
[d] Hitit University, Faculty of Arts and Sciences, Department of Chemistry, 19030, Corum, Turkey

ARTICLE INFO

Keywords:
Al/p-Si
Photodiode applications
Nicotinic acid
Nicotinamide
Metal complexes

ABSTRACT

Schottky type photodiodes have gained great interest due to their fast response to light. Various materials have been used to improve their efficiency behaviors as interlayers or electrodes. In this study, we synthesized Cu- and Mn-centered nicotinamide/nicotinic acid complexes and used them for Schottky type photodiode as interfacial layer. Thus, Al/Cu-complex/p-Si and Al/Mn-complex/p-Si metal semiconductor heterojunctions were fabricated by Al metal and p-Si semiconductor. The *I–V* and *I-t* analyses were employed to identify the fabricated devices under various light power intensities. The devices were evaluated according to various diode parameters such as series resistance, ideality factor and barrier height values obtained by *I–V* characteristics data from thermionic emission theory, Cheung and Norde techniques. Furthermore, various parameters of photodetection such as specific detectivity, photosensitivity and responsivity were calculated from the *I-t* measurements. The results reveal that heterojunctions can be employed for photodiode applications.

1. Introduction

Metal complexes are obtained by centering of metal by a ligand which can be neutral, anionic or cationic, and benzene-1,3,5-tricarboxylate, terephthalate, dicarboxylate succinate, 1,2,4,5-benzenetetracarboxylate, salicylates, nicotinamide, maleate etc. can be employed as ligand binder in these complexes [1–7]. To establish two- or three-dimensional network, molecules above the O or N atoms are composed being donor ligands. For supporting polymetric structures, the donor ligands make links between metal centers. These complexes can be used in sensors, catalysis and energy storage applications due to their excellent behaviors [8–14]. The performance of the metal complexes can be tested in photodetectors or photodiode applications [15,16].

When a metal and semiconductor contact each other correctly, ohmic or metallic contacts are occurred depending on their work functions [17,18]. While the metallic contacts are used in Schottky diodes, metal semiconductor field effect transistors (FETs) and Schottky transistors, the ohmic contacts are employed in almost all semiconductor devices such as transistors, p-n diodes, metal oxide FETs etc. to provide electrical transmission from semiconductor to external circuits [19–22]. Especially, in Schottky type photodiodes, various insulator, polymer or metal-oxide layers as interface materials are usually employed between the semiconductor and metal to control conductivity behaviors and to improve photodetection performance [23,24]. These interfacial layers also provide to adjust charge conduction, to stop leakage current and to passivate dangling bonds which causes trap levels for charge carries [25–27]. There are numerous studies to use metal complexes for photodetection applications in the literature. Argoni et al. synthesized neutral [M(R-dmet)2] bis(1,2-dithiolene) complexes with metal to fabricate metal-semiconductor-metal structure for photodetecting of light in the near infrared region [28]. Karabulut et al. employed organic Ru(II) complexes interfacial layer for metal-semiconductor Schottky type photodiode, and they obtained high photoresponse values [29]. We believe that the Cu and Mn centered nicotinamide/nicotinic acid complexes are potential to use as interfacial

* Corresponding author.
** Corresponding author.
E-mail addresses: adem.kocyigit@bilecik.edu.tr (A. Kocyigit), desrayildiz@hitit.edu.tr (D.E. Yıldız).

https://doi.org/10.1016/j.cap.2022.11.001
Received 30 July 2022; Received in revised form 26 October 2022; Accepted 2 November 2022
Available online 6 November 2022

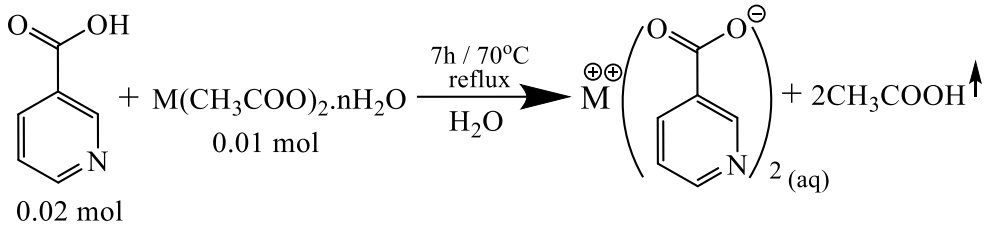

Scheme 1. Synthesis route of schematic reaction for metal cation-nicotinate salts.

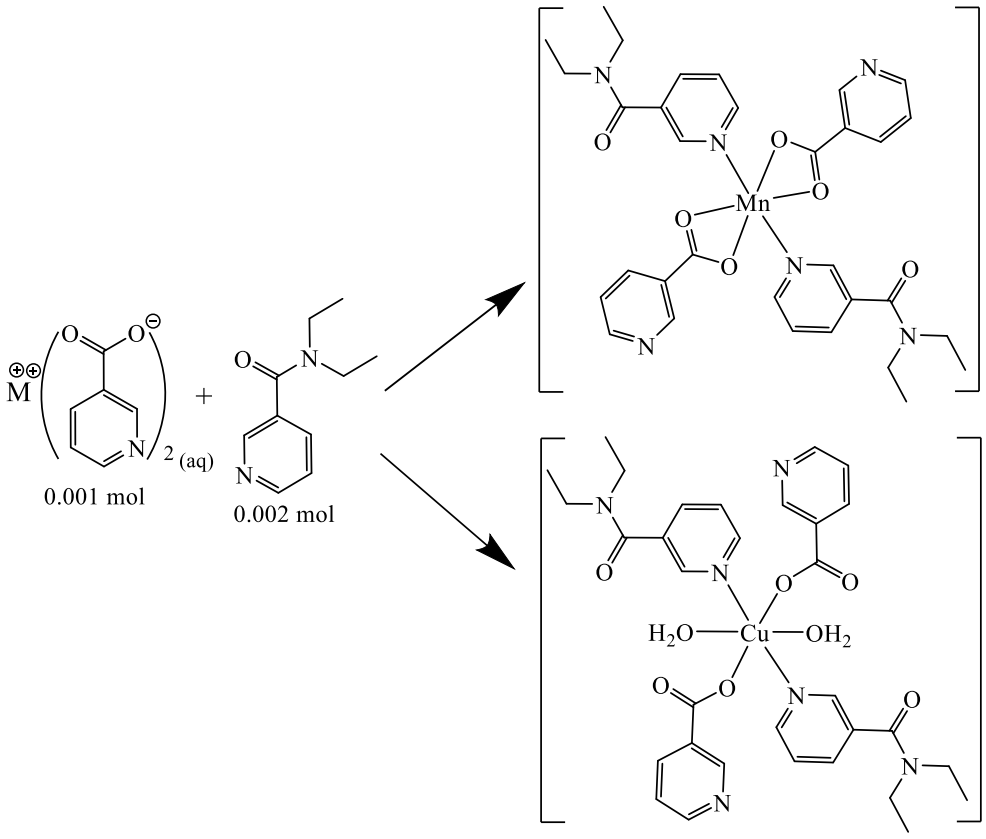

Scheme 2. Synthesis process of reaction schematic belonging to nicotinic acid centered with Mn(II) and Cu(II) metal cation/N,N-diethylnicotinamide mixed ligand complex.

layer for Schottky type photodiodes.

The high conductivity levels of metal cations in oxides or other salt compounds decrease to controllable low levels in complex structures with organic ligands. Electron mobility, which is effective in electrical conductivity, increases or decreases depending on external excitation (such as light, magnetic field or heat) in such complex structures. Therefore, in order to benefit from the specified properties of such complexes, the possibility of using them in photodiode studies has been preferred. Aim of this is to test and compare the nicotinamide/nicotinic acid complexes with the Cu and Mn metals according to photodiode performance for Schottky type photodetectors. For that aim, the Cu and Mn centered nicotinamide/nicotinic acid complexes which were called as Cu- and Mn-complexes were synthesized and used as interlayer for p-Si semiconductor and Al metal to fabricate efficient photodiode devices. Thus, Al/Cu-complex/p-Si and Al/Mn-complex/p-Si devices were fabricated and tested for changing light power intensity by *I-t* and *I–V* characteristics. The photodetector parameters were also studied for metal centered nicotinamide/nicotinic acid complexes interlayers depending on wavelengths for the first time according to our best knowledge.

2. Experimental

2.1. Synthesis

$C_6H_5NO_2$ (Nicotinic acid), $C_{10}H_{14}N_2O$ (N,N-diethylnicotinamide), $Mn(CH_3COO)_2{\cdot}4H_2O$ (manganese acetate) and $Cu(CH_3COO)_2{\cdot}H_2O$ (copper acetate) to be used for the synthesis of coordination compounds were purchased from Sigma-Aldrich. Distilled water was used as a solvent in the reactions. For the synthesis of metal complex compounds, metal nicotinate salts were obtained by reacting the acetate salts of the relevant metal cations with nicotinic acid separately (Scheme 1). A 100 mL distilled water used to solve 2.462 g and 0.02 mol of nicotinic acid, and 0.01 mol of manganese acetate (2.451 g) or copper acetate (1.997 g) salts were added to obtained aquas solution. The reaction was continued in the reflux mechanism at 70 °C with continuous stirring until the odor of acetic acid remained in the environment. The absence of acetic acid odor was interpreted as an indication that the reagents were completely converted to metal nicotinate salt. N,N-diethylnicotinamide (3.565 g) solutions (50 ml distilled water) were included separately at a ratio of 0.02 mol into the Mn(II) and Cu(II) metal nicotinate solutions in aqueous

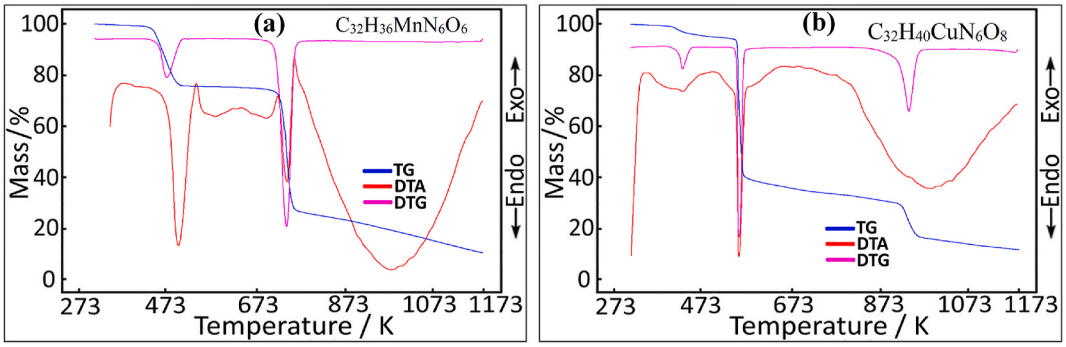

Fig. 1. a) DTA and TG-DTG curves of the $[Mn(C_6H_4NO_2)_2(C_{10}H_{14}N_2O)_2]$ and b) $[Cu(C_6H_4NO_2)_2(C_{10}H_{14}N_2O)_2(H_2O)_2]$ complexes.

Table 1
Metal-nicotinate/N,N-diethylnicotinamide mixed ligands' thermal analysis data.

Complexes		Temp. Range (°C)	DTA_{max} (°C)	Removed Groups	Mass Loss (%)		Remain Product (%)		Decomp. Product	Colour
					Exp.	Calc.	Exp.	Calc.		
$[Mn(C_6H_4NO_2)_2(C_{10}H_{14}N_2O)_2]$										pale-white
$C_{32}H_{36}MnN_6O_6$	1	167–225	190	2 $N(C_2H_5)$	22.72	22.00				
655.61 g/mol	2	420–491	461	2 C_5H_4N 2 C_6H_4NO	55.78	56.19				
	3	493–871	664	CO; CO_2	9.57	10.99	11.93	10.82	MnO	black
$[Cu(C_6H_4NO_2)_2(C_{10}H_{14}N_2O)_2(H_2O)_2]$										dark-blue
$C_{32}H_{40}CuN_6O_8$	1	95–230	151	2 H_2O	4.92	5.14				
700.25 g/mol	2	235–377	295	2 $C_5H_4N_{(nic)}$ 2 $C_5H_{10}NO$	51.12	50.91				
	3	380–882	698	2 $C_5H_4N_{(dena)}$ CO; CO_2	31.85	32.59	12.11	11.36	CuO	black

nic: nicotinate and *dena*: N,N-diethylnicotinamide

solution (Scheme 2)]. The resulting total reaction solutions were stirred at 50 °C for about 5 h on a magnetic stir hot plate [30–32]. The final solutions were covered with a perforated paraffin film and left until crystal formation into a beaker. After 20–25 days, pale white crystals for Mn(II) and dark blue for Cu(II) of the respective metal cation complexes were collected.

2.2. Device fabrications

99.999% pure aluminum was used as both metal and ohmic contacts of the Al/Cu-complex/p-Si and Al/Mn-complex/p-Si heterojunctions. A one-side polished p-type Si wafer semiconductor, 7.3×10^{15} cm^{-3} carrier concentrations, 1–10 Ω cm resistivity and (100) crystalline orientation, was employed for fabrication of heterojunctions. Firstly, the wafer was divide into 2×1 cm^2 slices and then cleaned in an ultrasonic cleaner by acetone, distilled water and isopropanol. Secondly, HF:H_2O (1:10) solution was prepared and used to remove natural SiO_2 layers from the slices for only 30 s, and they were dried by nitrogen. Thirdly, the slices were immediately transferred into a thermal evaporator to obtain a 200 nm thick Al ohmic contacts on the back surfaces, and ohmic contacts were formed by thermal annealing at 450 °C for 5 min. Fourthly, the Cu- and Mn-complex solution were coated onto the slices by spin coating system at 3000 rpm for 30 s and dried softly at 80 °C for 1 h. The thicknesses of the Cu- and Mn-complex layer were obtained as 172 nm and 186 nm, respectively by a Veeco Dektak 150 stylus profilometer. Fifthly, the thermal evaporator was employed again to deposit Al metallic contacts (100 nm) on the Cu- and Mn-complex film layers by hole array masks. Thus, the Al/Cu-complex/p-Si and Al/Mn-complex/p-Si heterojunctions were successfully fabricated for photodiode applications. To confirm results, many test have been carried out by many same junctions in the experiments to eliminate errors.

2.3. Characterization

Chemical composition compositions of the complexes were found with the Korloerva 1106 model elemental analyzer. The Shimadzu TG60H instrument was employed for TGA analysis. The UV-3600i Plus Shimadzu Spectrophotometer was used for UV–Vis spectrometer measurements. The fabricated heterojunction devices were characterized by *I–V* and *I-t* measurements for changing light power illumination as well as various wavelengths with Fytronix FY-7000.

3. Results and discussion

3.1. Structural properties

Chemical composition and chemical formula of the complex molecules were confirmed by chemical composition analysis data. For the Mn (II) complex ($C_{32}H_{36}MnN_6O_6$), experimentally was calculated as C:58.17%; H:6.07%; N:12.77%, C:58.62%; theoretically was calculated as H:5.53%; N:12.82%. For the Cu(II) complex ($C_{32}H_{40}CuN_6O_8$), experimentally was calculated as C:54.65%; H:6.22%; N:11.93%, theoretically was calculated as C:54.89%; H:5.76%; N:12.00%. The thermal analysis curves of the metal cation complexes are shown in Fig. 1a and b. Table 1 shows also data summarizing of the degradation steps and products obtained from the curves. Depending on the differentiated format of Mn and Cu metal cation complexes, differences in thermal decomposition steps were also noted. Due to the absence of any hydrate molecules in the Mn(II) structure, bonding via two neutral and monodentate N,N-diethylnicotinamide (*dena*) and two mono-anionic bidentate coordinated carboxylate oxygens coordinated from the –N group in the pyridine ring of the metal's octahedral coordination geometry. The degradation of the complex started with the degradation of organic ligands, and it was determined that the nitrogen-bound diethyl groups of

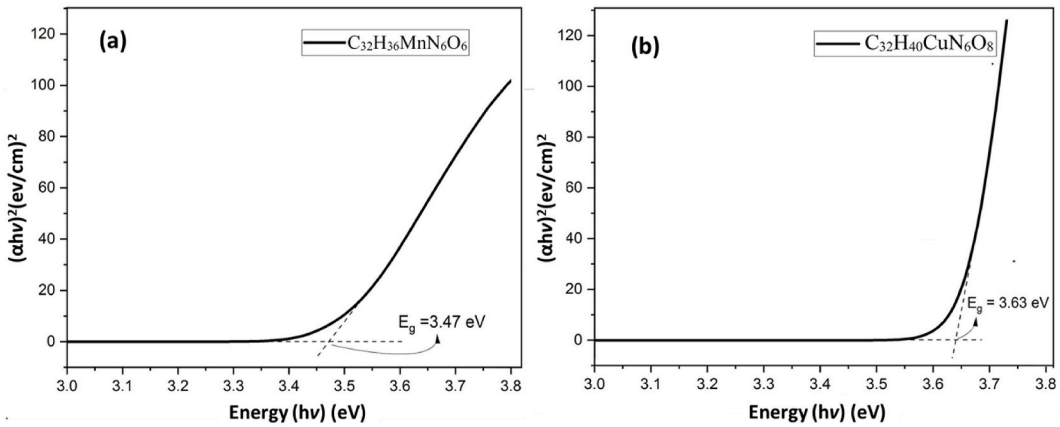

Fig. 2. E_g curves of a) Mn(II) and b) Cu(II) complexes.

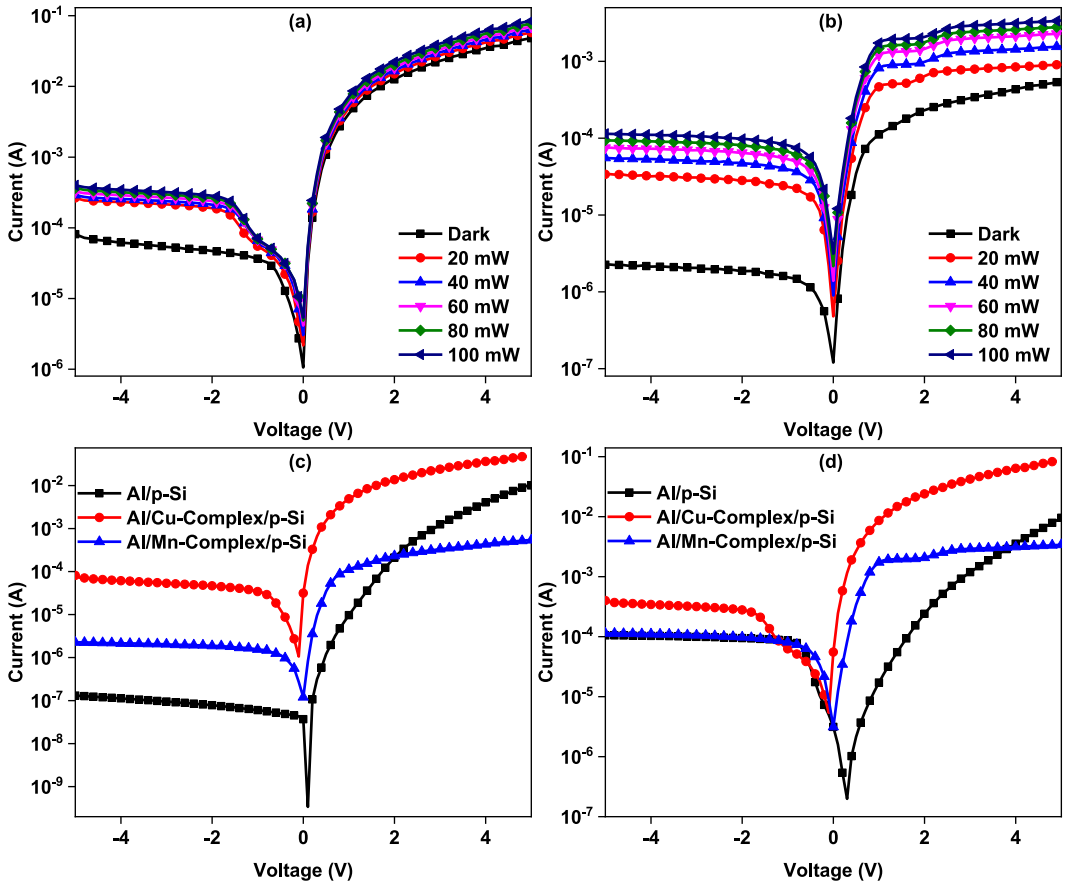

Fig. 3. ln*I-V* graphs of a) Al/Cu-complex/p-Si and b) Al/Mn-complex/p-Si devices for various light intensities. Comparison the Al/p-Si (reference), Al/Cu-complex/p-Si and Al/Mn-complex/p-Si devices c) in dark and d) 100 mW/cm^2 illumination conditions.

the neutral and *dena* ligands were removed first (exp. 22.72%; theo. 22.00%). The experimental and theoretical weight losses of the next degradation step indicated the fragmentation of the remaining portions of the *dena* ligands and the pyridine rings of the nicotinate ligands (exp. 55.78%; theo. 56.19%). In the final decomposition step, the organic residue was completely burned by forming CO and CO_2 gases, and MnO oxide stayed as the final residue production. Coordination geometry for Cu(II) metal cation-containing structure can be thought to be in an octahedral structure with two nicotinate ligands bonded mono-anionic monodentate to the metal via acidic oxygen, two *dena* ligands showing neutral monodentate bonding from the pyridine ring nitrogen, and two coordinated aqua molecules. This suggested that the degradation of the complex continued with the removal of the two crystal waters in the structure, and then the decomposition of the organic structure was similar to the Mn(II) complex (Table 1). The complex decomposed completely at 882 °C and CuO oxide remains as a residual product. Both oxides remaining as residue products were black in color, and the experimental weight losses were approximately 1% lower than the calculated weight losses which were interpreted as the thermal decomposition being carried out in an inactive nitrogen medium. Some carbon of organic ligands in the structure cannot be completely burned due to the lack of enough combustible oxygen and accumulated on

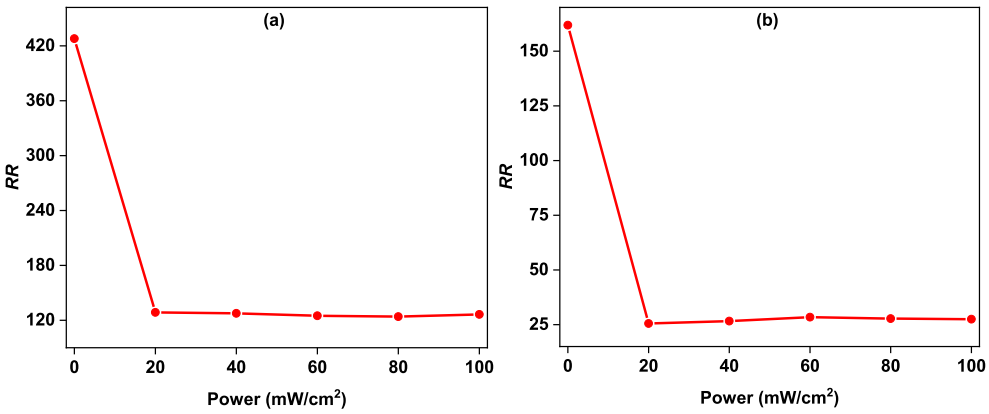

Fig. 4. *RR* profiles of a) Al/Cu-complex/p-Si and b) Al/Mn-complex/p-Si devices for varying power intensity.

Table 2
The device specifications of Al/Cu-complex/p-Si and Al/Mn-complex/p-Si heterojunctions.

Device Interlayer	Saturation Current (I_0)	n (I–V)	n Cheung	Φ_b (I–V)	Φ_b Norde	Φ_b Cheung	R_s Norde	R_s Cheung	R_s Cheung
		–	–	(eV)	(eV)	(eV)	(Ω)	(Ω ($H(I)$))	(Ω ($d\ln(I)$))
Cu-Complex	5.12×10^{-6}	2.61	2.86	0.58	0.60	0.55	110.68	189.43	202.25
Mn-Complex	1.74×10^{-7}	2.62	2.62	0.66	0.69	0.66	3471.50	4696.89	5688.49

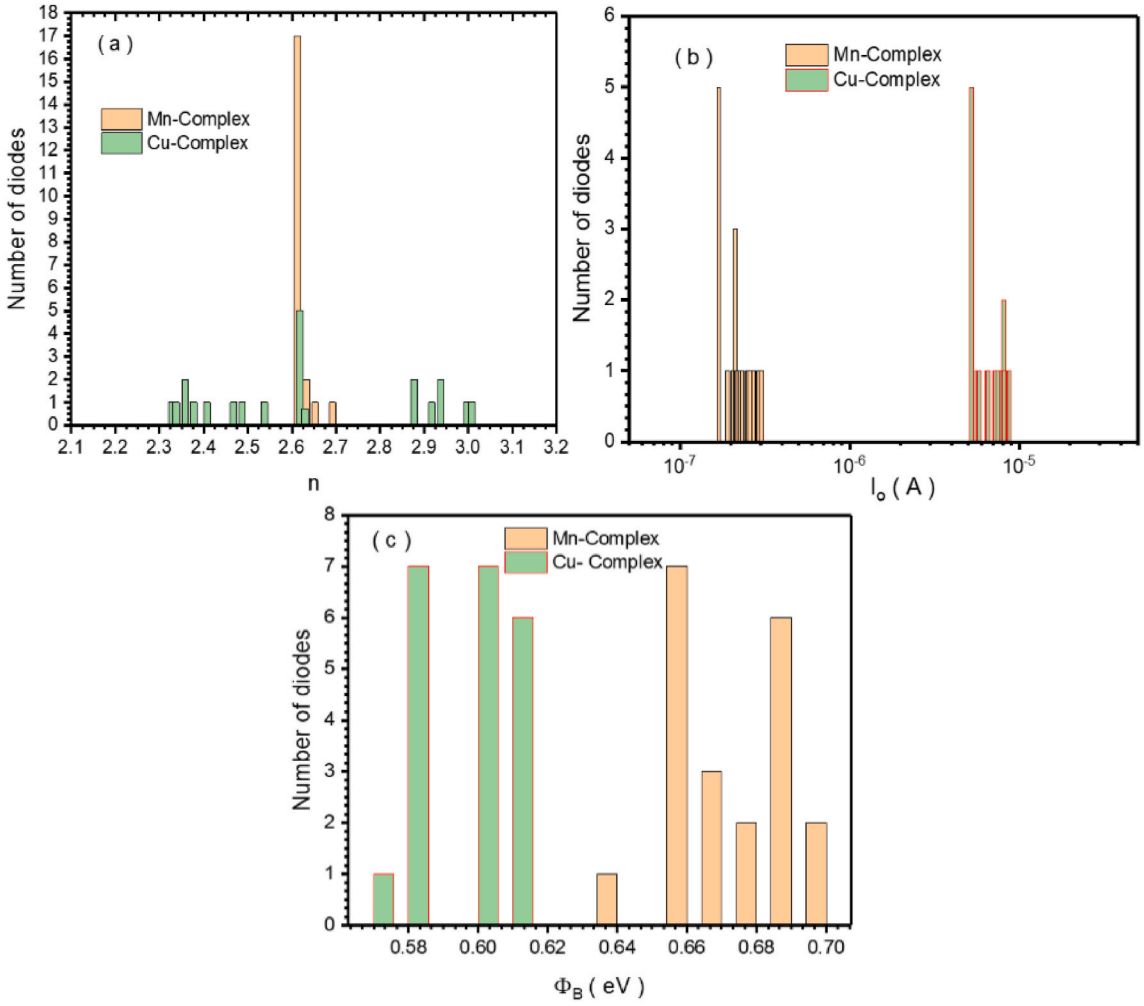

Fig. 5. The statistical analysis of a) n, b) Io and c) Φ_b for 21 Al/Cu-complex/p-Si and Al/Mn-complex/p-Si heterojunctions from dark I–V data.

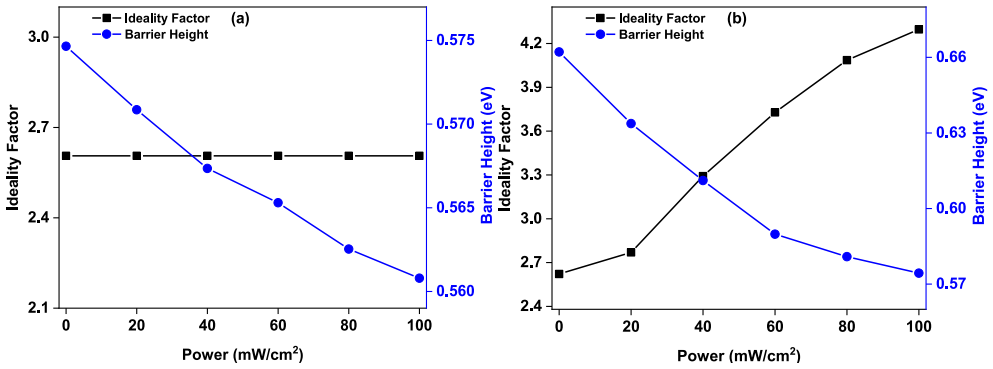

Fig. 6. n - Φ_b graphs of a) Al/Cu-complex/p-Si and b) Al/Mn-complex/p-Si heterojunctions for changing light power intensity.

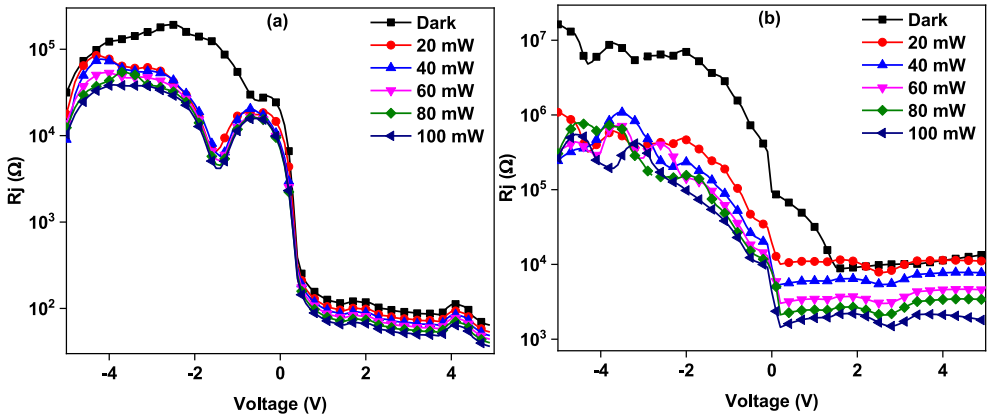

Fig. 7. R_j-V graphs of a) Al/Cu-complex/p-Si and b) Al/Mn-complex/p-Si heterojunctions for changing intensity of light power.

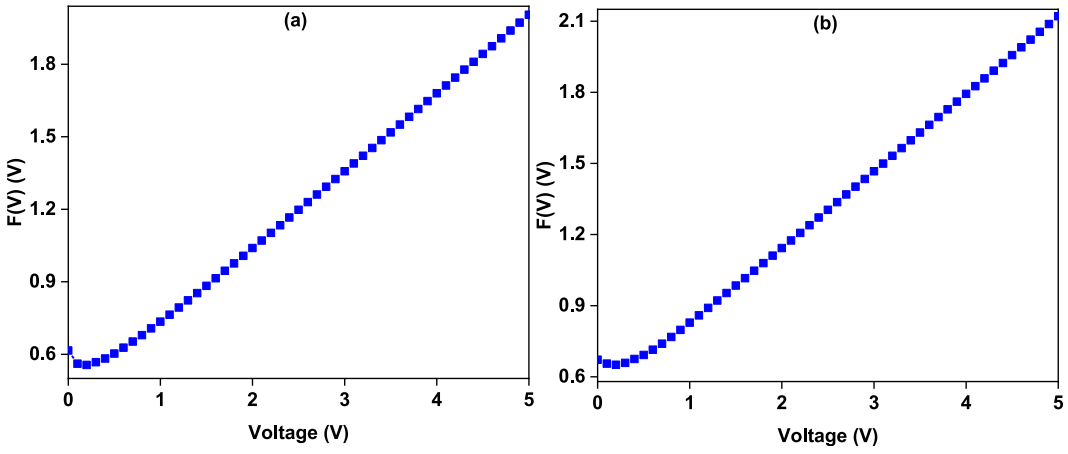

Fig. 8. Norde function graphs of a) Al/Cu-complex/p-Si and b) Al/Mn-complex/p-Si heterojunctions.

residual oxides in the form of carbonized carbon.

The UV–Visible spectrometer was used to obtain band gap (E_g) curves. E_g curves of the Mn(II) and Cu(II) complexes have been exhibited in Fig. 2a and b, respectively. While the Mn(II) complex has band gap value of 3.47 eV, the Cu(II) complex has 3.63 eV. These values are extremely high for solar cell devices, but the complexes can be used for UV photodetector devices.

3.2. Electrical properties

According to increasing of light power intensity from dark to 100 mW/cm^2, I–V characteristics of the Al/Cu-complex/p-Si and Al/Mn-complex/p-Si heterojunctions are indicated in Fig. 3a and b, respectively. The devices clearly revealed increase of the photocurrent both at reverse and forward biases with increasing light power. The devices can be performed for photodetection applications because of increase at the currents with increasing light power [33,34]. While the Al/Cu-complex/p-Si has almost 10 times increase at the current at reverse biases from dark to highest light power (100 mW/cm^2), the Al/Mn-complex/p-Si device has almost 100 times increase. This difference can be attributed to structure of metal complexes for various centered metals. Furthermore, the Al/Mn-complex/p-Si device has increase at current values almost 10 times at forward biases with increasing light power. The I–V characteristic levels of the Al/p-Si

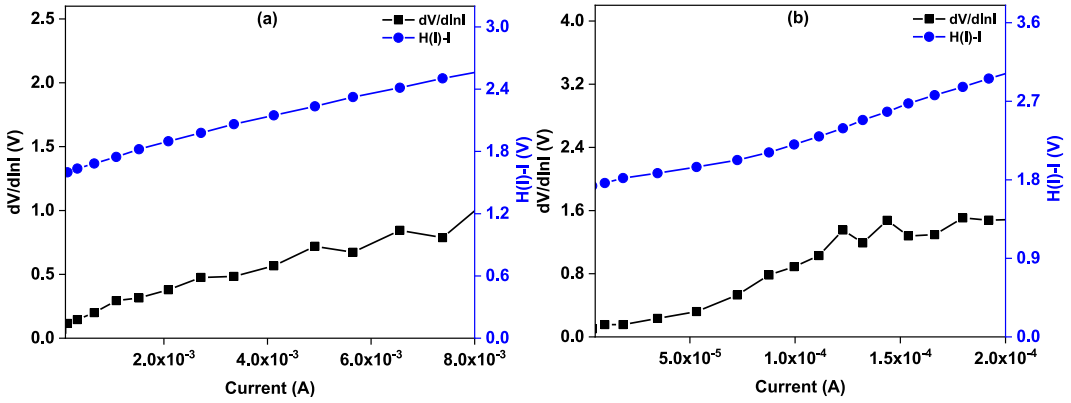

Fig. 9. Cheung graphs of a) Al/Cu-complex/p-Si and b) Al/Mn-complex/p-Si heterojunctions.

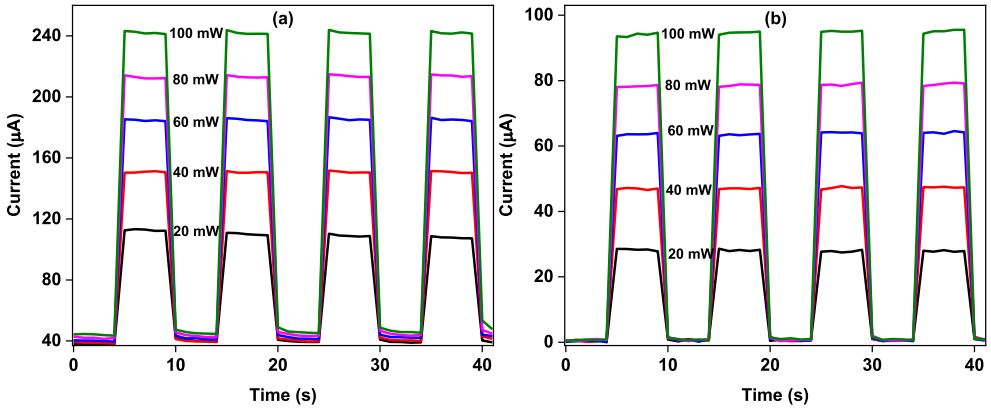

Fig. 10. *I-t* graphs of a) Al/Cu-complex/p-Si and b) Al/Mn-complex/p-Si heterojunctions for changing intensity of light power.

(reference), Al/Cu-complex/p-Si and Al/Mn-complex/p-Si devices for dark and 100 mW/cm^2 values are compared and given in Fig. 3c and d. The complex interlayers caused to increase dark current due to increasing charge carriers at reverse biases. While the Al/Cu-complex/p-Si device has highest forward and reverse currents in both light illumination and dark, the Al/Mn-complex/p-Si device shows higher jump at the current by increasing light intensity than Al/Cu-complex/p-Si device. These results clearly approve the better detection light property of the Al/Mn-complex/p-Si. Some of researchers studied electrical properties of the complex structure in the literature between metals or metal and semiconductor devices. Temirci *et al.* synthesized 1-Amino-5-benzoyl-4-phenyl-1H pyrimidine-2-thione as ligand (N-APTH), and the N-APTH was mixed with $Cu(CH_3COO)_2{\cdot}2H_2O$ to obtain Cu(II) complexes [35]. Both N-APTH and Cu(II) complexes were employed to obtain Al/Cu(II)Complex/Cu and Al/Ligand (N-APTH)/Cu devices. The devices evaluated as rectifier not photodiodes. They also did not used a semiconductor layer such as silicon or germanium. Ghosh *et al.* synthesized hexadentate Schiff base ligand (H_2L) from 2,2-dimethyl-1,3-propanediamine with 5-bromo-3-methoxy-salicylaldehyde in acetonitrile [36]. Then, they used Co $(CH_3CO_2)_2{\cdot}4H_2O$ and NaN_3 to obtain a polymeric complex of $[(N_3)CoLNa(N_3)]n$. The complex structure was used as interfacial layer between indium tin oxide (ITO) and Al to fabricate ITO/complex/Al device. The device was tested under 100 mW/cm^2 light illumination and dark. The outcomes revealed that the device can be employed for photodetection applications. In this study, we used p-Si as semiconductor and nicotinamide as ligand to obtain Cu- and Mn complexes based Schottky type photodiodes. In our previous studies on the nicotinamide ligands with various metals has been exhibited good photodiode behaviors [15,16,37–39].

The Al/Cu-complex/p-Si and Al/Mn-complex/p-Si heterojunctions exhibited photodetection behavior via good rectification ratio (*RR*) values. The *RR* values show the diode efficiency for conducting at forward biases and stopping current at reverse biases [40]. They were calculated for every light power intensity value from *I–V* measurements. The *RR* value changes of the Al/Cu-complex/p-Si and Al/Mn-complex/p-Si heterojunctions are indicated in Fig. 4a and b, respectively for ±3 V. The *RR* values decreased with 20 mW/cm^2 light power and stayed constant by changing of other power intensity values.

The diode parameters of the metal-semiconductor heterojunctions such as barrier height (Φ_b), series resistance (R_s), saturation current (I_o) and ideality factor (n) can be determined to evaluate the performance of them. According to literature, these parameters are determined by Norde, Cheung, thermionic emission theory, Werner methods etc. [41–44]. Thermionic emission theory uses second region of ln*I-V* plot for forward biases to calculate I_o, n and Φ_b values. While the slope of the second region provides to calculate n value, y-intercept yield the Φ_b value of the device. The detailed formula and calculation processes can be found in the literature [45]. The I_o, Φ_b and n values were calculated both Al/Cu-complex/p-Si and Al/Mn-complex/p-Si heterojunctions from dark *I–V* data (Fig. 3c) and all values of both devices are tabulated and compared in Table 2. The statistical analysis was carried out to investigate the reliability of the electrical parameters determined for both Al/Cu-complex/p-Si and Al/Mn-complex/p-Si heterojunctions. The statistical accuracy of the electrical parameters for both Al/Cu-complex/p-Si and Al/Mn-complex/p-Si heterojunctions presented in Table 2 can be seen in Fig. 5. For this, 21 separate diodes for both heterojunctions were produced, and the n, I_o *and* Φ_b parameters were determined by using dark *I–V* measurements. Fig. 5a, 5b and 5c shows the statistics of n, Φ_b and I_o parameters depending on the number

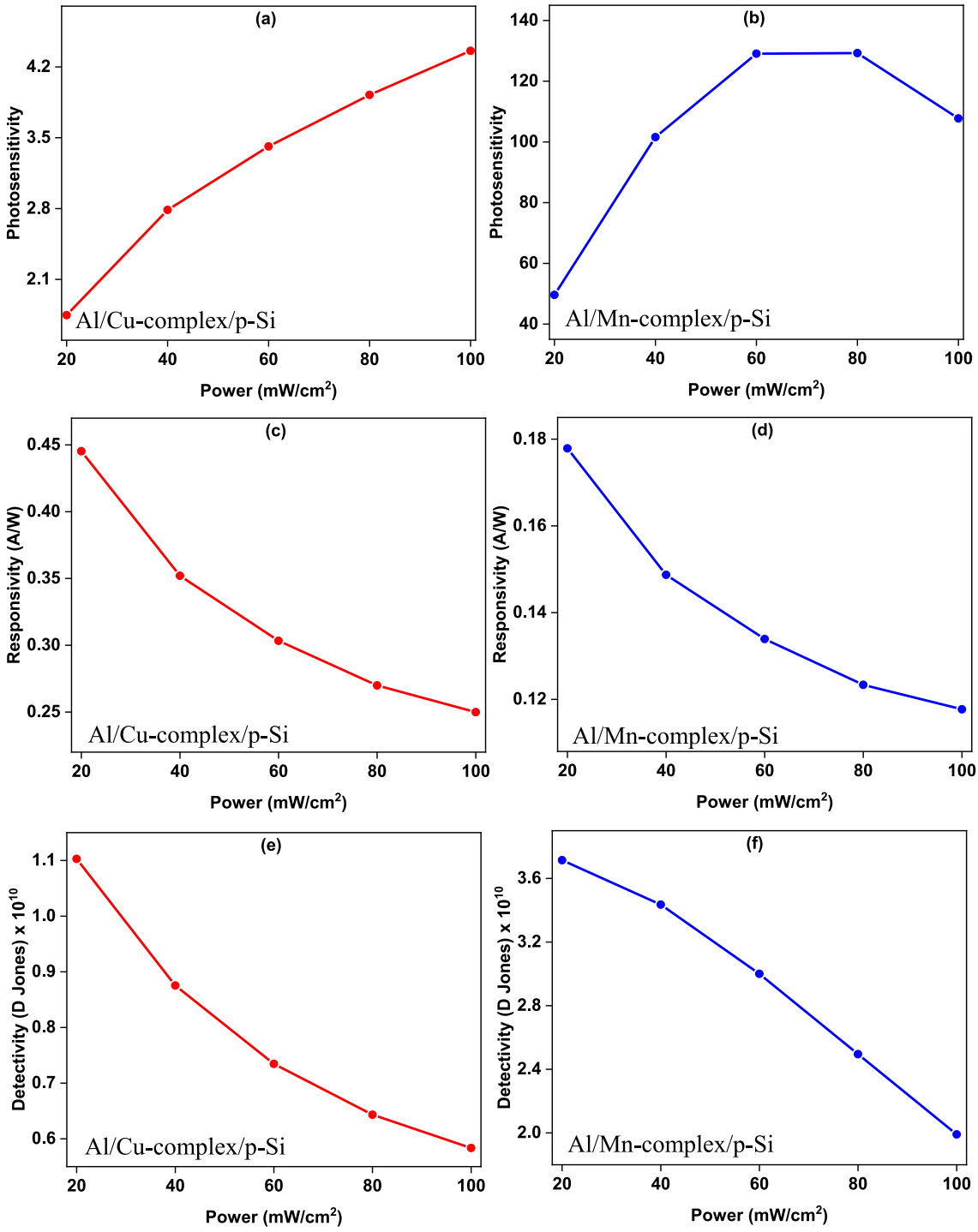

Fig. 11. a,b) Photosensitivity c,d) responsivity and e,f) specific detectivity profiles of Al/Cu-complex/p-Si and Al/Mn-complex/p-Si heterojunctions for changing illumination power.

of diodes, respectively. The n value is 2.61 for 17 Al/Mn-complex/p-Si diodes and 2.62 for 5 Al/Cu-complex/p-Si diodes as seen Fig. 5a. The I_o value is 1.74×10^{-7} A for 5 Al/Mn-complex/p-Si and 5.12×10^{-6} A for 5 Al/Cu-complex/p-Si as seen Fig. 5b. In addition, the Φ_b value is 0.66 eV for 7 Al/Mn-complex/p-Si and 0.69 eV for 6 Al/Mn-complex/p-Si diodes. In the case of Al/Cu-complex/p-Si diodes, Φ_b values are 0.58 eV and 0.60 eV for 7 each diodes, and 0.61 eV in 6 diodes. The results confirm reliability of the fabricated heterojunctions.

The Φ_b and n values were calculated both Al/Cu-complex/p-Si and Al/Mn-complex/p-Si heterojunctions from I–V data depending on illumination conditions. Their changing profile with illumination conditions have been shown in Fig. 6a and b for Al/Cu-complex/p-Si and Al/Mn-complex/p-Si, respectively. The Φ_b values of the both devices slightly decreased by increasing illumination intensity power due to raising of carrier amounts and decreasing depletion layer [46]. In the case of Al/Cu-complex/p-Si device, n values did not change with increasing intensity of light power, but they raised for the Al/Mn-complex/p-Si device. It means that Al/Cu-complex/p-Si structure did affect from the light increase. Both devices has high ideality factor than unity due to interfacial layer and interface states effect or

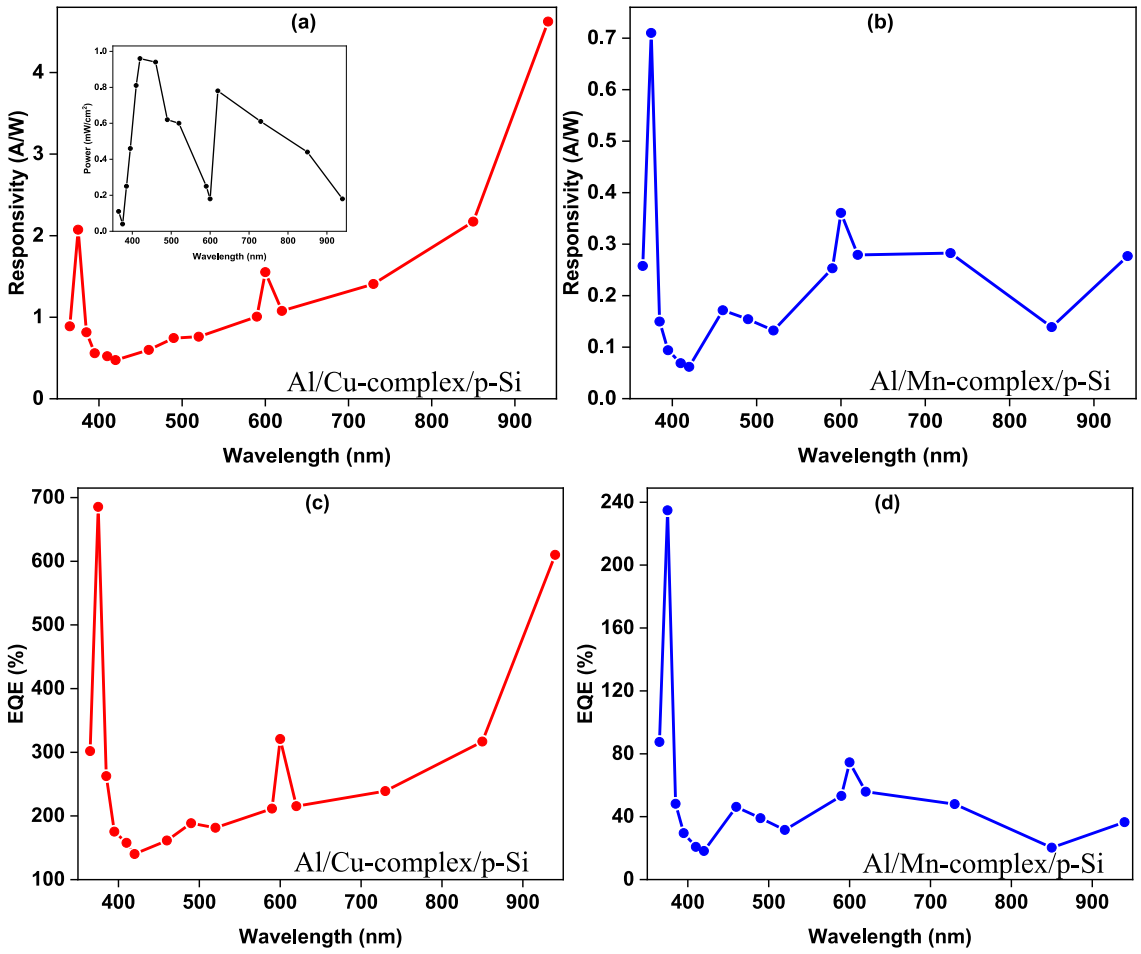

Fig. 12. a,b) Responsivity and c,d) external quantum efficiency profiles of Al/Cu-complex/p-Si and Al/Mn-complex/p-Si heterojunctions for changing illumination wavelength.

barrier inhomogeneities [47,48].

These kinds of metal-semiconductor junctions have a junction resistance (R_j) which is obtained from I–V data by $R_j = dV/dI$ formula. The R_j has two parts: series resistance in the case of forward biases and shunt resistance (R_{sh}) in the case of reverse biases [49]. For a good device performance, the high R_{sh} and low R_s values are aimed. Fig. 7a and b displays R_j versus voltage graphs of the Al/Cu-complex/p-Si and Al/Mn-complex/p-Si heterojunctions, respectively. Both devices have decreasing R_{sh} and R_s profiles by increment light intensity because of raising charge carriers. While the R_{sh} values of the Al/Cu-complex/p-Si and Al/Mn-complex/p-Si devices were verified as around 10^5 Ω and 10^7 Ω under dark, R_s values were obtained 10^2 Ω and 10^4 Ω levels, respectively. These values are acceptable for photodetection of light.

Norde proposed another method to calculate barrier height and series resistance values from I–V data for whole forward bias region [50]. The technique uses Norde function to calculate related parameters, and their formulas can be found in the literature [51]. Norde function plots of the Al/Cu-complex/p-Si and Al/Mn-complex/p-Si heterojunctions are exhibited in Fig. 8a and b, respectively, and normal Norde function profiles have been seen from figures. The obtained Φ_b and R_s values are displayed in Table 2 for both devices. There can be seen slightly higher Φ_b values than thermionic Φ_b values due to approximation differences between two techniques [52].

Cheung also proposed another method to reveal diode specifications by using Cheung functions ($H(I)$ and $dV/d\ln(I)$) plots depending on current [53,54]. The slopes of both functions give series resistances which should be closed each other. The y-intercept of the $H(I)$ and $dV/d\ln(I)$ functions provide to determine the Φ_b and n values, respectively. Cheung graphs of Al/Cu-complex/p-Si and Al/Mn-complex/p-Si heterojunctions are displayed Fig. 9a and b, and obtained Φ_b, n and R_s values are shown in Table 2. These calculated values are good agreement with calculated from other techniques. Trivial differences can be attributed to again approximation diversity.

The photoconducting and photoresponse mechanism of an optoelectonic devices can be determined by photocurrent transient or current on-off measurements. This measurement provides to determine the prophotosensitivity, responsivity and detectivity values based on the varying intensity of power [55–58]. Fig. 10a and b exhibit the photocurrent transient characteristics of Al/Cu-complex/p-Si and Al/Mn-complex/p-Si heterojunctions for increasing light power intensities at 2V biases. Both devices revealed almost linearly current increase with increasing light power.

The current-transient measurements were employed to calculate detector behaviors of Al/Cu-complex/p-Si and Al/Mn-complex/p-Si heterojunctions. The photocurrent(I_p), photosensitivity(K), responsivity(R) and specific detectivity(D^*) and external quantum efficiency (EQE) equations are given by next formulas, respectively [59,60].

$$I_p = I_{light} - I_{dark} \tag{1}$$

$$K = \frac{I_p}{I_{dark}} \tag{2}$$

$$R = \frac{I_p}{PA} \tag{3}$$

$$D^* = R\sqrt{\frac{A}{2qI_{dark}}} \tag{4}$$

$$EQE = R\frac{hc}{q\lambda_{nm}} \tag{5}$$

where A is the effective detector area, and P shows power density. The h, c and λ_{nm} indicate Planck constant, light speed and incident light wavelength in nm, subsequently.

The photosensitivity profile of Al/Cu-complex/p-Si and Al/Mn-complex/p-Si heterojunctions are displayed in Fig. 11a and b depending on light intensity of power, respectively. While the Al/Cu-complex/p-Si device almost has linear photosensitivity profile with raising of power intensity, the Al/Mn-Complex/p-Si device has some discrepancy from linearity after 60 mW/cm^2 light power illumination intensity. Both devices have pretty high photoresponsivity with illumination. Figs. 11c and d indicate responsivity changes of Al/Cu-complex/p-Si and Al/Mn-complex/p-Si heterojunctions, respectively for changing illumination power intensity. The devices have a low responsivity value, and they slightly dropped by increment of illumination power energy. The specific detectivity versus light power intensity profiles of Al/Cu-complex/p-Si and Al/Mn-complex/p-Si devices are exhibited Fig. 11e and f, respectively. The D^* values have decreasing profile for both devices. The obtained D^* values are 10^{10} Jones level, and they are high enough for a kind of optoelectronic device.

Responsivity and external quantum efficiency values were discussed according to changing illumination wavelength values. A homemade LED system was built for illumination of Al/Cu-complex/p-Si and Al/Mn-complex/p-Si heterojunctions by different wavelengths. However, all LED's have different power intensity. Power intensity change profile of the LED system is indicated inset of Fig. 12a. Figs. 12a and b exhibit wavelength dependent responsivity profile of the Al/Cu-complex/p-Si and Al/Mn-complex/p-Si heterojunctions, subsequently. The external quantum efficiency (*EQE*) profiles of the Al/Cu-complex/p-Si and Al/Mn-complex/p-Si heterojunctions are displayed in Fig. 12c and d, respectively.

4. Conclusion

Nicotinamide/nicotinic acid were used to synthesize Cu and Mn metal centered complexes by chemically and used as interfacial layer in among p-Si and Al to fabricate Al/Cu-complex/p-Si and Al/Mn-complex/p-Si metal semiconductor heterojunctions. The *I-t* and *I–V* measurements were used to characterize the devices by under dark and different illumination power intensity of light. While the n values of Al/Cu-complex/p-Si and Al/Mn-complex/p-Si heterojunctions were calculated as 2.61 and 2.62, respectively, the Φ_b values were accounted as 0.58 eV and 0.66 eV from theory of thermionic emission. The Norde and Cheung techniques also were used to verify the values of the Φ_b, n and R_s. The various detector specifications such as photosensitivity, responsivity and specific detectivity were depicted by *I-t* measurements. The obtained detector parameters reveal that the devices exhibit good photodiode and photodetector performance according to results, and they can be improved for optoelectronic applications.

Declaration of competing interest

The authors declare that they have no known competing financial interests or personal relationships that could have appeared to influence the work reported in this paper.

Acknowledgement

This work was supported by Selçuk University BAP office with the research Project Number of 21401015.

References

[1] J. Kim, U. Lee, B.K. Koo, Synthesis and 1D Chain crystal structure of zinc(II) terephthalate complex: [Zn(tp)(py)(H2O)]n, Bull. Kor. Chem. Soc. 31 (2010) 1743–1746, https://doi.org/10.5012/bkcs.2010.31.6.1743.
[2] B.K. Koo, J. Kim, U. Lee, Synthesis and crystal structures of di- and tetra-nuclear dicarboxylate-bridged copper(II) complexes, Inorg. Chim. Acta. 363 (2010) 1760–1766, https://doi.org/10.1016/j.ica.2010.02.032.
[3] Yong Bok Go, Xiqu Wang, V. Ekaterina, Anokhina, A.J. Jacobson*, Influence of the reaction temperature and pH on the coordination modes of the 1,4-benzenedicarboxylate (BDC) ligand: a case study of the NiII(BDC)/2,2'-Bipyridine system, Inorg. Chem. 44 (2005) 8265–8271, https://doi.org/10.1021/IC050644D.
[4] H. Xu, R. Wang, Y. Li, Zn2Na2(BDC)3·(DMF)2·(μ-H2O)2: rare 3D channel-structures with pendant DMF constructed by carboxyl group bridging heterometallic ions, J. Mol. Struct. 688 (2004) 1–3, https://doi.org/10.1016/J.MOLSTRUC.2003.07.003.
[5] N. Hao, Y. Li, E. Wang, E. Shen, C. Hu, L. Xu, Hydrothermal synthesis and crystal structure of an infinite 1D ladderlike metal-organic compound: [Cu2(btec)(2,2′-bipy)2] ∞ (btec = 1,2,4,5-benzenetetracarboxylate), J. Mol. Struct. 697 (2004) 1–8, https://doi.org/10.1016/S0022-2860(03)00349-1.
[6] B.K. Koo, Synthesis and crystal structures of MN(II)- and NI(II)-dicarboxylate complexes with 1,10-phenanthroline, Bull. Kor. Chem. Soc. 33 (2012) 2299–2304, https://doi.org/10.5012/bkcs.2012.33.7.2299.
[7] O.M. Yaghi, H. Li, C. Davis, D. Richardson, T.L. Groy, Synthetic strategies, structure patterns, and emerging properties in the chemistry of modular porous solids, Acc. Chem. Res. 31 (1998) 474–484, https://doi.org/10.1021/ar970151f.
[8] N. Sari, E. Kahraman, B. Sari, A. Özgün, Synthesis of some polymer-metal complexes and elucidation of their structures, J. Macromol. Sci. Part A Pure Appl. Chem. 43 (2006) 1227–1235, https://doi.org/10.1080/10601320600737484.
[9] Z.S. Şahin, M. Demir, T. Yıldırım, Ö. Yurdakul, D.A. Köse, Novel mixed ligand complexes of Co(II), Ni(II), Cu(II), and Zn(II) with 1,10-phenanthroline and acesulfame. Synthesis, structural analysis and hydrogen adsorption study, Int. J. Hydrogen Energy 46 (2021) 27631–27642, https://doi.org/10.1016/j.ijhydene.2021.06.026.
[10] Ö. Yurdakul, Z.S. Şahin, D.A. Köse, O. Şahin, F. Akkurt, Novel monoanionic diphenate-nicotinamide/N,N-diethylnicotinamide complexes of NiII, ZnII. Synthesis, structural investigations and hydrogen adsorption study, J. Mol. Struct. 1218 (2020), 128514, https://doi.org/10.1016/j.molstruc.2020.128514.
[11] C.N.R. Rao, S. Natarajan, R. Vaidhyanathan, Metal carboxylates with open architectures, Angew. Chem., Int. Ed. 43 (2004) 1466–1496, https://doi.org/10.1002/anie.200300588.
[12] J. Kim, U. Lee, B.K. Koo, 1D chain crystal structure of copper(II) oxalate containing a 4,4'-bipyridine and 1,10-phenanthroline ligands: [Cu2(ox)(4,4'-bpy) (phen)2](NO3)2, Bull. Kor. Chem. Soc. 31 (2010) 487–490, https://doi.org/10.5012/bkcs.2010.31.02.487.
[13] O.V. Nesterova, A.J.L. Pombeiro, D.S. Nesterov, Novel H-bonded synthons in copper supramolecular frameworks with aminoethylpiperazine-based ligands. Synthesis, structure and catalytic activity, Materials 13 (2020) 1–19, https://doi.org/10.3390/ma13235435.
[14] M.S.A. Abdel-Mottaleb, E.H. Ismail, Transition metal complexes of mixed bioligands: synthesis, characterization, DFT modeling, and applications, J. Chem. 2019 (2019), https://doi.org/10.1155/2019/3241061.
[15] H.H. Gullu, D.E. Yıldız, D.A. Kose, M. Yıldırım, Si-based photosensitive diode with novel Zn-doped nicotinate/nicotinamide mixed complex interlayer, Mater. Sci. Semicond. Process. 147 (2022), 106750, https://doi.org/10.1016/j.mssp.2022.106750.
[16] A. Kocyigit, M. Yıldırım, D.A. Kose, D.E. Yıldız, Synthesize and characterization of Co-complex as interlayer for Schottky type photodiode, Polym. Bull. (2022) 1–20, https://doi.org/10.1007/s00289-021-04021-0.
[17] L.M. Porter, J.R. Hajzus, Perspectives from research on metal-semiconductor contacts: examples from Ga 2 O 3 , SiC, (nano)diamond, and SnS, J. Vac. Sci. Technol. 38 (2020), 031005, https://doi.org/10.1116/1.5144502.
[18] S.S. Li, Metal–Semiconductor Contacts, in: Semicond. Phys. Electron., Springer, 2006, pp. 284–333, https://doi.org/10.1007/0-387-37766-2_10. New York, NY, New York, NY.
[19] A.A. Noroozi, Y. Abdi, A graphene/Si Schottky diode for the highly sensitive detection of protein, RSC Adv. 9 (2019) 19613–19619, https://doi.org/10.1039/c9ra03765a.
[20] J. Kwon, J.-Y. Lee, Y.-J. Yu, C.-H. Lee, X. Cui, J. Hone, G.-H. Lee, J.S. Kang, J. Baik, H.J. Shin, S.C. Hong, S.Y. Lee, D. Jena, W. Choi, K. Kim, T. Low, P. Kim, J. Hone, Thickness-dependent Schottky barrier height of MoS2 field-effect transistors, Nanoscale 9 (2017) 6151–6157, https://doi.org/10.1039/C7NR01501A.
[21] M. Jang, Scalability of Schottky barrier metal-oxide-semiconductor transistors, Nano Converg 3 (2016) 11, https://doi.org/10.1186/s40580-016-0071-0.
[22] H.S. Lee, K. Choi, J.S. Kim, S. Yu, K.R. Ko, S. Im, Coupling two-dimensional MoTe2 and InGaZnO thin-film materials for hybrid PN junction and CMOS inverters, ACS Appl. Mater. Interfaces 9 (2017) 15592–15598, https://doi.org/10.1021/acsami.7b02838.
[23] M. Yilmaz, Y. Demir, S. Aydogan, M.L. Grilli, Density functional theory calculations of pinus brutia derivatives and its response to light in a Au/n–Si device, Energies 14 (2021), https://doi.org/10.3390/en14237983, 7983.
[24] B. Ezhilmaran, A. Patra, S. Benny, S. M.R., A. V.V., S.V. Bhat, C.S. Rout, Recent developments in the photodetector applications of Schottky diodes based on 2D materials, J. Mater. Chem. C 9 (2021) 6122–6150, https://doi.org/10.1039/d1tc00949d.

[25] N. Suntornwipat, S. Majdi, M. Gabrysch, K.K. Kovi, V. Djurberg, I. Friel, D. J. Twitchen, J. Isberg, A valleytronic diamond transistor: electrostatic control of valley currents and charge-state manipulation of NV centers, Nano Lett. 21 (2021) 868–874, https://doi.org/10.1021/acs.nanolett.0c04712.
[26] İ. Taşçıoğlu, W.A. Farooq, R. Turan, Ş. Altındal, F. Yakuphanoglu, Charge transport mechanisms and density of interface traps in MnZnO/p-Si diodes, J. Alloys Compd. 590 (2014) 157–161, https://doi.org/10.1016/J.JALLCOM.2013.12.043.
[27] A. Kaya, E. Marıl, Ş. Altındal, İ. Uslu, The comparative electrical characteristics of Au/n-Si (MS) diodes with and without a 2% graphene cobalt-doped Ca3Co4Ga0.001Ox interfacial layer at room temperature, Microelectron. Eng. 149 (2016) 166–171, https://doi.org/10.1016/J.MEE.2015.10.012.
[28] M.C. Aragoni, M. Arca, F.A. Devillanova, F. Isaia, V. Lippolis, A. Mancini, L. Pala, G. Verani, T. Agostinelli, M. Caironi, D. Natali, M. Sampietro, First example of a near-IR photodetector based on neutral [M(R-dmet)2] bis(1,2-dithiolene) metal complexes, Inorg. Chem. Commun. 10 (2007) 191–194, https://doi.org/10.1016/j.inoche.2006.10.019.
[29] A. Karabulut, A. Dere, O. Dayan, A.G. Al-Sehemi, Z. Serbetci, A.A. Al-Ghamdi, F. Yakuphanoglu, Silicon based photodetector with Ru(II) complexes organic interlayer, Mater. Sci. Semicond. Process. 91 (2019) 422–430, https://doi.org/10.1016/j.mssp.2018.11.035.
[30] D.A. Köse, F. Akkurt, O. Şahin, O. Büyükgüngör, Synthesis and structural characterization of a binuclear mixed-ligand (Salicylate and N,N-diethylnicotinamide) nickel(II) complex, its magnetic properties. [Ni2(μ-Sal)4 (Dena)2]H2O, J. Chin. Chem. Soc. 61 (2014) 1326–1332, https://doi.org/10.1002/jccs.201400292.
[31] O. Şahin, O. Büyükgüngör, D.A. Köse, B. Zümreoglu-Karan, H. Necefoglu, Catena-Poly[[[triaquacobalt(II)]-μ-2,6-dioxo-1,2,3,6- tetrahydropyrimidine-4-carboxylato (2-)] 1.72-hydrate], Acta Crystallogr. Sect. C Cryst. Struct. Commun. 62 (2006) m513–m515, https://doi.org/10.1107/S010827010603767X/BG3013ISUP2. HKL.
[32] Ö. Yurdakul, D.A. Köse, O. Şahin, D. Özer, Mn(II) and Co(II) mixed-ligand coordination compounds with acesulfame and 3-aminopyridine: synthesis and structural properties, J. Coord. Chem. 74 (2021) 1168–1180, https://doi.org/10.1080/00958972.2021.1888083.
[33] B. Ezhilmaran, A. Patra, S. Benny, S. M.R., A. V.V., S.V. Bhat, C.S. Rout, Recent developments in the photodetector applications of Schottky diodes based on 2D materials, J. Mater. Chem. C 9 (2021) 6122–6150, https://doi.org/10.1039/d1tc00949d.
[34] G. Dushaq, M. Rasras, Planar multilayered 2D GeAs Schottky photodiode for high-performance visible-near-infrared photodetection, ACS Appl. Mater. Interfaces 13 (2021) 21499–21506, https://doi.org/10.1021/acsami.1c01773.
[35] C. Temirci, M. Gülcan, K. Goksen, M. Sönmez, Ohmic and rectifier properties of Al/Ligand(N-APTH) and Al/Cu(II)Complex contacts, Microelectron. Eng. 87 (2010) 2282–2287, https://doi.org/10.1016/j.mee.2010.03.004.
[36] K. Ghosh, S. Sil, P.P. Ray, J. Ortega-Castro, A. Frontera, S. Chattopadhyay, Photosensitive Schottky barrier diode behavior of a semiconducting Co(iii)-Na complex with a compartmental Schiff base ligand, RSC Adv. 9 (2019) 34710–34719, https://doi.org/10.1039/c9ra06354d.
[37] B. Barış, M. Yıldırım, S. Karadeniz, A. Karabulut, A. Kose, D.E. Yıldız, Effect of illumination on electrical characteristics of Au/Mn-complex/n-Si photodiode structures, J. Mater. Sci. Mater. Electron. 33 (2022) 2631–2642, https://doi.org/10.1007/s10854-021-07469-y.
[38] A. Karabulut, D.E. Yıldız, D.A. Köse, M. Yıldırım, Photosensing performances of heterojunctions-based photodiodes with novel complex interlayers, Mater. Sci. Semicond. Process. 146 (2022), 106647, https://doi.org/10.1016/j.mssp.2022.106647.
[39] S. Karadeniz, D.E. Yıldız, H.H. Gullu, D.A. Kose, A.A. Hussaini, M. Yıldırım, Dark and illuminated electrical characteristics of Schottky device with Zn-complex interface layer, J. Mater. Sci. Mater. Electron. 2022 (2022) 1–15, https://doi.org/10.1007/S10854-022-08664-1.
[40] H.N. Tran, T.A. Bui, G.K. Reeves, P.W. Leech, J.G. Partridge, M.S.N. Alnassar, A. S. Holland, Optimising the rectification ratio of Schottky diodes in n-SiC and n-Si by TCAD, MRS Adv 1 (2016) 3655–3660, https://doi.org/10.1557/adv.2016.343.
[41] A. Di Bartolomeo, F. Giubileo, G. Luongo, L. Iemmo, N. Martucciello, G. Niu, M. Fraschke, O. Skibitzki, T. Schroeder, G. Lupina, Tunable Schottky barrier and high responsivity in graphene/sinanotip optoelectronic device, 2D Mater. 4 (2017), 015024, https://doi.org/10.1088/2053-1583/4/1/015024.
[42] W.A. Farooq, E. Elgazzar, A. Dere, O. Dayan, Z. Serbetci, A. Karabulut, M. Atif, A. Hanif, Photoelectrical characteristics of novel Ru(II) complexes based photodiode, J. Mater. Sci. Mater. Electron. 30 (2019) 5516–5525, https://doi.org/10.1007/s10854-019-00845-9.
[43] A. Kocyigit, İ. Karteri, I. Orak, S. Uruş, M. Çaylar, The structural and electrical characterization of Al/GO-SiO2/p-Si photodiode, Phys. E Low-Dimensional Syst. Nanostructures. 103 (2018) 452–458, https://doi.org/10.1016/j.physe.2018.06.006.
[44] A. Kocyigit, I. Orak, Z. Çaldıran, A. Turut, Current–voltage characteristics of Au/ZnO/n-Si device in a wide range temperature, J. Mater. Sci. Mater. Electron. 28 (2017) 17177–17184, https://doi.org/10.1007/s10854-017-7646-3.
[45] N.A. Al-Ahmadi, Metal oxide semiconductor-based Schottky diodes: a review of recent advances, Mater. Res. Express 7 (2020), 032001, https://doi.org/10.1088/2053-1591/ab7a60.
[46] S.M. Sze, Physics of Semiconductor Devices, edition, vol. 2, Wiley, Newyork, 1981.
[47] A. Kirsoy, M.A. Afrailov, A. Asimov, B. Kucur, The electrical properties of Au/P3HT/n-GaAs Schottky barrier diode, in: Acta Phys. Pol. A, Polska Akademia Nauk, 2015, pp. 170–173, https://doi.org/10.12693/APhysPolA.128.B-170.
[48] H. Kacus, Y. Sahin, S. Aydogan, U. Incekara, M. Yilmaz, Co/aniline blue/silicon sandwich hybrid heterojunction for photodiode and low-temperature applications, J. Sandw. Struct. Mater. 23 (2021) 2547–2565, https://doi.org/10.1177/1099636220909946.
[49] A. Tursucu, S. Aydogan, A. Kocyigit, A. Ozmen, M. Yilmaz, Investigation the performance of Cr-doped ZnO nanocrystalline thin film in photodiode applications, JOM (J. Occup. Med.) 74 (2022) 777–786, https://doi.org/10.1007/s11837-021-05096-w.
[50] H. Norde, A modified forward I-V plot for Schottky diodes with high series resistance, J. Appl. Phys. 50 (1979) 5052–5053, https://doi.org/10.1063/1.325607.
[51] A. Turut, Determination of barrier height temperature coefficient by Norde's method in ideal Co/n-GaAs Schottky contacts, Turk. J. Phys. 36 (2012) 235–244, https://doi.org/10.3906/fiz-1103-8.
[52] A. Koçyiğit, A. Sarılmaz, T. Öztürk, F. Ozel, M. Yıldırım, A Au/CuNiCoS4/p-Si photodiode: electrical and morphological characterization, Beilstein J. Nanotechnol. 12 (2021) 984–994, https://doi.org/10.3762/bjnano.12.74.
[53] T.T. Anh Tuan, D.-H. Kuo, Characteristics of RF reactive sputter-deposited Pt/SiO2/n-InGaN MOS Schottky diodes, Mater. Sci. Semicond. Process. 30 (2015) 314–320, https://doi.org/10.1016/j.mssp.2014.10.021.
[54] M. Yilmaz, A. Kocyigit, B.B. Cirak, H. Kacus, U. Incekara, S. Aydogan, The comparison of Co/hematoxylin/n-Si and Co/hematoxylin/p-Si devices as rectifier for a wide range temperature, Mater. Sci. Semicond. Process. 113 (2020), 105039, https://doi.org/10.1016/j.mssp.2020.105039.
[55] M. Shkir, M.T. Khan, I.M. Ashraf, A. Almohammedi, E. Dieguez, S. AlFaify, High-performance visible light photodetectors based on inorganic CZT and InCZT single crystals, Sci. Rep. 9 (2019) 1–9, https://doi.org/10.1038/s41598-019-48621-3.
[56] C. Li, J. Li, Z. Li, H. Zhang, Y. Dang, F. Kong, High-performance photodetectors based on nanostructured perovskites, Nanomaterials 11 (2021) 1038, https://doi.org/10.3390/nano11041038.
[57] H.H. Gullu, D.E. Yildiz, A. Kocyigit, M. Yıldırım, Electrical properties of Al/PCBM: ZnO/p-Si heterojunction for photodiode application, J. Alloys Compd. 827 (2020), 154279, https://doi.org/10.1016/j.jallcom.2020.154279.
[58] D.E. Yildiz, H.H. Gullu, A. Sarilmaz, F. Ozel, A. Kocyigit, M. Yildirim, Dark and illuminated electrical characteristics of Si-based photodiode interlayered with CuCo5S8 nanocrystals, J. Mater. Sci. Mater. Electron. 31 (2020) 935–948, https://doi.org/10.1007/s10854-019-02603-3.
[59] J.M. Wu, W.E. Chang, Ultrahigh responsivity and external quantum efficiency of an ultraviolet-light photodetector based on a single VO2 microwire, ACS Appl. Mater. Interfaces 6 (2014) 14286–14292, https://doi.org/10.1021/am503598g.
[60] D. Banerjee, I.M. Asuo, A. Pignolet, S.G. Cloutier, Low-cost photodetector architectures fabricated at room-temperature using nano-engineered silicon wafer and sol-gel TiO2 – based heterostructures, Sci. Rep. 9 (2019) 1–9, https://doi.org/10.1038/s41598-019-54481-8.